Energy 60 (2013) 492–500

Contents lists available at ScienceDirect

Energy

journal homepage: www.elsevier.com/locate/energy

A comparison of lead-acid and lithium-based battery behavior and capacity fade in off-grid renewable charging applications

Elena M. Krieger, John Cannarella, Craig B. Arnold*

Department of Mechanical and Aerospace Engineering, Princeton University, Princeton, NJ 08544, USA

ARTICLE INFO

Article history:
Received 21 January 2013
Received in revised form
2 August 2013
Accepted 17 August 2013
Available online 18 September 2013

Keywords:
Off-grid renewables
Lead-acid
Lithium-ion
Capacity fade
Wind
Variable charge

ABSTRACT

The effects of variable charging rates and incomplete charging in off-grid renewable energy applications are studied by comparing battery degradation rates and mechanisms in lead-acid, LCO (lithium cobalt oxide), LCO-NMC (LCO-lithium nickel manganese cobalt oxide composite), and LFP (lithium iron phosphate) cells charged with wind-based charging protocols. Poor pulse charge acceptance, particularly for long pulses, contributes to incomplete charging and rapid degradation of lead-acid cells due to apparent high rates of sulphation and resistance growth. Partial charging and pulse charging, common lead-acid stressors in off-grid applications, are found to have little if any effect on degradation in the lithium-based cells when compared to constant current charging. These cells all last much longer than the lead-acid cells; the LFP batteries show the greatest longevity, with minimal capacity fade observed after over 1000 cycles. Pulse charge acceptance is found to depend on pulse length in lead-acid and LFP cells, but not in LCO and LCO-NMC cells. Excellent power performance and consistent voltage and power behavior during cycling suggest that LFP batteries are well-suited to withstand the stresses associated with off-grid renewable energy storage and have the potential to reduce system lifetime costs.

1. Introduction

Of the 1.3 billion people in the world without access to electricity [1], 85% live in rural areas where grid expansion can be prohibitively expensive [2]. Those who do have electricity away from the grid typically rely on diesel generators, renewable energy systems, or some combination thereof [3,4]. Diesel users may experience widely variable prices and potential loss of supply in politically, economically or environmentally unstable areas, whereas renewable energy systems can both bring energy to those far from the grid and provide energy independence to protect users from this volatility [5]. Without a connection to the grid, energy storage is a crucial component for ensuring reliability of these standalone renewable energy systems [5,6]. These systems primarily rely on lead-acid batteries to store electricity, in spite of many recent advances in battery technology [7,8]. Low initial costs and widespread availability make lead-acid cells attractive, but they tend to degrade quickly in off-grid systems and require frequent replacement, contributing to high system lifetime costs [9,10]. The clear need for better energy storage in off-grid renewable systems has led some researchers to pursue alternate energy storage technologies such as flywheels or hydrogen [11,12]. However, these demands may also be met by improving lead-acid charging technique or by replacing these cells with a more suitable battery chemistry.

The characteristic features of off-grid renewable energy systems, including highly variable charging powers, deep cycling, partial cycling, and infrequent full charge [13,14] are known stressors for lead-acid battery systems: long periods at low SOC (state-of-charge) with infrequent full charge increase sulphation and acid stratification [13–15]. Studies of capacity fade in off-grid renewable systems focus almost exclusively on lead-acid batteries, although lithium-based battery technologies, including LCO (lithium cobalt oxide), LCO-NMC (LCO-lithium nickel manganese cobalt oxide composite) and, more recently, LFP (lithium iron phosphate) chemistries, have been shown to have much longer cycle lives. Manufacturer-supplied specification sheets show that lead-acid batteries can typically be expected to last only 200-300 standard cycles at 100% DOD (depth-of-discharge) before degrading to 80% capacity (the standard measure of end-of-life). Lithium-ion cells fade to 80% capacity after 500+ cycles [16]. LFP cells can retain over 95% capacity after 1000 cycles [17]. Even in more complex systems, LFP batteries show little degradation: in studies simulating electric vehicle utilization, these cells retain more than 90% of their initial capacity after well more than 1000 cycles [17,18]. Power fade in LFP cells has only been reported at powers higher

* Corresponding author. Tel.: +1 617 258 1089; fax: +1 617 258 5877.
E-mail address: cbarnold@princeton.edu (C.B. Arnold).

0360-5442/$ – see front matter © 2013 Elsevier Ltd. All rights reserved.
http://dx.doi.org/10.1016/j.energy.2013.08.029

than those typical of off-grid systems [19]. While lithium battery control systems [20] and basic operational performance [21,22] have been described for renewable and hybrid systems, work evaluating aging and degradation has only begun to probe lithium-based electrode response to photovoltaic inputs at lab scale [23].

Lithium-ion chemistries have many features that may make them attractive for off-grid applications. Lithium-ion cells are typically rated for much higher charge and discharge powers than lead-acid cells, allowing them to absorb high pulses of generated power or meet sudden power demands. Lithium-ion cells show less degradation at partial SOC than at full charge [17], have good performance at relatively high DOD, and do not require full recharge to prevent degradation, meaning that the stress of infrequent full charges found in off-grid systems may actually be a benefit. Although they appear well-suited for the intermittency of renewable energy systems, long-term lithium-ion battery performance is not much studied in such applications. Here we will compare degradation rates and mechanisms in lead-acid, LCO, LCO-NMC, and LFP cells in a stand-alone wind system.

In this study we will focus on several specific features of aging in renewable energy systems. Few battery aging studies examine off-grid wind systems [24]; most research addresses off-grid solar [9,10,23,25]. Consequently, we base our charging protocol on the output of a small wind turbine. We also modify the time steps and maximum power of the wind profile to elucidate how power distribution, frequency of power oscillations, and other variables affect performance and degradation; this approach will allow us to apply our results to other variable charging systems. We focus solely on variable *charging*, and keep discharge rates constant, to isolate the components of variable charging which affect degradation. This paper is structured as follows: in Section 3 we describe our experimental approach to evaluating the impact of wind variability on battery degradation; in Section 4 we look at capacity fade and power fade in the batteries and use differential capacity analysis to study degradation mechanisms; finally, we conclude with a brief comparison of the economics of each battery chemistry and discuss the implications for using lithium-based cells in off-grid renewable applications.

2. Background

The characterization and prediction of battery aging in renewable energy systems is very complicated due to the many aging processes involved, the path dependence of some aging mechanisms, and large variations in charging and usage between different systems [13,15]. Furthermore, battery degradation studies typically rely on accelerated aging tests due to time constraints [16]. As a result, many aging tests focus primarily on a limited set of stressors. Existing studies on battery charging current and variability show varied and at times contradictory results. In field studies of off-grid wind systems, wind-based charging is found to result in very low system efficiency due to the poor pulse charge acceptance of lead-acid batteries, resulting in losses of up to 75% of wind-generated energy [26,27]. Okazaki et al. found that alternating currents from 0.1 to 4000 Hz superimposed over a low constant charge/discharge current had little impact on lead-acid batteries [28], while Lam et al. found that charging using pulses <1 s greatly increased cycle life [29]. Kirchev et al. showed that high frequency pulses reduce overpotential on the lead negative electrode, but low frequencies (50 mHz) increase hydrogen evolution in the cell [30]. The ideal pulse frequency for the positive electrode is reported to be about 1 Hz, the resonant time of the electrochemical double layer [31]. Pavlov et al. found high charging currents increase cycle life in lead-acid batteries [32], whereas Lam et al. found that increasing current greatly decreases cycle life unless using a pulsed current [29]. Pulse charge in lithium-based cells has been reported to have mixed impacts as well. In LFP batteries, pulse charge is found to negatively impact battery performance by contributing to overpotential, with decreasing capacity and efficiency associated with longer pulses and higher deviation of the root mean square current from the mean [33]. In lithium-ion batteries pulse charging at 1000 Hz is found to improve efficiency and battery life [34]. In this study, we focus on lower frequencies than typically studied in order to capture the characteristic variability in renewables.

3. Experimental

3.1. Wind profile

The wind profile used in this study is derived from the output of a small (150 W) wind turbine located on the roof of the Princeton University engineering quadrangle in Princeton, NJ. We collect 600 s of output current data at a resolution of 1 s, resulting in a 1 s "time step." This sequence of output current ranges from 0 A to 6 A and averages 1.4 A, shown in Fig. 1. We scale these values for each battery so that the average charging current is $C/5$ for any cell, and the maximum current pulse is roughly $0.8C$, where C is the current at which the battery would fully discharge in an hour. The 600 s wind profile is repeated until the battery is fully charged. We choose this approach in lieu of using a longer data set to ensure that a similar charging protocol is used over the entire test life, rather than charging with only the first section of a long data set as capacity fade increases.

We modify the wind profile for some tests to assess how different features of the variable current profile impact degradation. The 1 s resolution of the original profile changes at most every second, or at a 1 Hz frequency. In order to evaluate the frequency response of the system, we re-scaled the 1 s time step. To create a "low-frequency wind profile" every time step was multiplied by 10 s, leaving the y-values (the magnitude of the output current) fixed. We modified the profile in this way to also create profiles with time steps of 0.1 s and 0.5 s, charging at an oscillation frequency of 10 Hz and 2 Hz, respectively. This approach allows us to determine if capacity fade is affected by the frequency of the oscillations, the power distribution, or both.

3.2. Battery test procedure

Battery testing is performed on a Maccor Series 4000 multi-channel battery tester in ambient room temperature (approximately 23 °C). Four battery chemistries are tested: lithium cobalt oxide, LCO-lithium nickel manganese cobalt oxide composite, lithium iron phosphate and lead-acid. All battery cells under test are purchased commercially available cells. The six lead-acid cells used here are VRLA (valve-regulated lead-acid) batteries rated 6 V 4.5 Ah. VRLA cells are selected instead of flooded cells due to their recommended usage in applications with partial cycling at low states of charge [13,35]. The five LCO cells and six LCO-NMC cells are both rated with a nominal voltage of 3.7 V and a capacity of

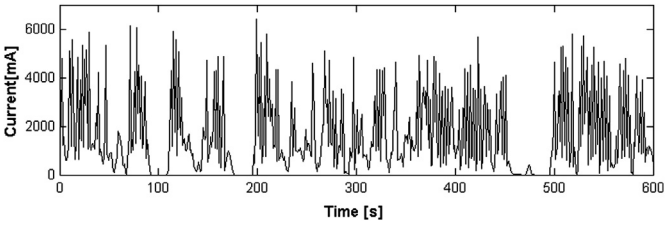

Fig. 1. Current output from a 150 W wind turbine used in aging tests.

Table 1
Battery charging protocols.

	Profile type	Time step	Frequency	Chemistries tested
Control	Constant charge	N/A	N/A	All
Modified	Standard wind charge	1 s	1 Hz	Lead-acid, LCO, LFP
	Low-frequency wind charge	10 s	0.1 Hz	Lead-acid, LCO, LFP
	Medium-frequency wind charge	0.5 s	2 Hz	LCO-NMC
	High-frequency wind charge	0.1 s	10 Hz	LCO-NMC

2.2 Ah. The six LFP cells are rated with a nominal voltage of 3.2 V and capacity of 2.0 Ah.

All batteries initially undergo three characterization cycles consisting of a CC–CV (constant current–constant voltage) charge at a *C*/3 rate, 5 min rest, and constant *C*/3 discharge followed by another 5 min rest. The initial C-rate is based on the battery's rated capacity, although during aging cycles the lead-acid C-rate is re-scaled to the initial measured capacity, which is lower than rated. Voltage ranges used are those specified by the manufacturer: 5.1 V–7.45 V for the VRLA cells; 3.0 V–4.2 V for the LCO and LCO-NMC cells; and 2.0 V–3.65 V for the LFP cells. Each battery is also charged a fourth time using the CC–CV protocol and discharged with 10 s pulses at incremental states of charge to derive internal resistance. During the aging tests, full capacity and resistance tests are performed after every 50 cycles. These tests follow the protocol for the characterization cycles, consisting of one full CC–CV charge and constant *C*/3 discharge as described to measure full capacity, and one resistance test cycle as described above.

Three primary cycling protocols are used to study battery degradation. The *standard wind* profile consists of repeating the 600 s wind profile until the battery's pre-determined voltage limit is reached, resting for 5 min, and discharging at *C*/3 until the discharge voltage limit is reached, followed by another 5 min rest. The *low-frequency wind* profile substitutes the modified wind profile with 10 s time steps but otherwise follows identical procedure. The *constant charge* profile consists of a constant *C*/5 charge to the voltage limit and *C*/3 discharge separated by 5 min rests. Two lead-acid, two LCO and two LFP cells are cycled according to each of these three protocols, followed by capacity tests after every 50 cycles.

The LCO-NMC batteries are tested using a different set of profiles than the other chemistries to probe battery response at time scales closer to the double layer response time. Two cells are charged according to the constant current profile described above. Two cells are charged with a *high-frequency wind* (10 Hz) protocol using a compressed wind profile with 0.1 s time steps. Two more cells are tested with a *medium-frequency wind* (2 Hz) protocol using a wind profile compressed to 0.5 s steps. A summary of the charge profiles and tests is provided in Table 1.

None of the batteries are charged with a constant voltage step, except during capacity tests, to ensure that such a step does not obfuscate the effects of variable charging; the batteries are therefore only partially charged during the cycling tests, simulating the intermittency of full charge seen in the field. The impact of such incomplete charge will be discussed later. In order to complete the study in a reasonable amount of time, we employ a few techniques to speed degradation: we discharge batteries 100% and charge batteries at currents higher than average for most off-grid applications. This approach is expected to slightly overemphasize degradation mechanisms induced by high powers and depth-of-discharge, but allows us to accelerate the aging process.

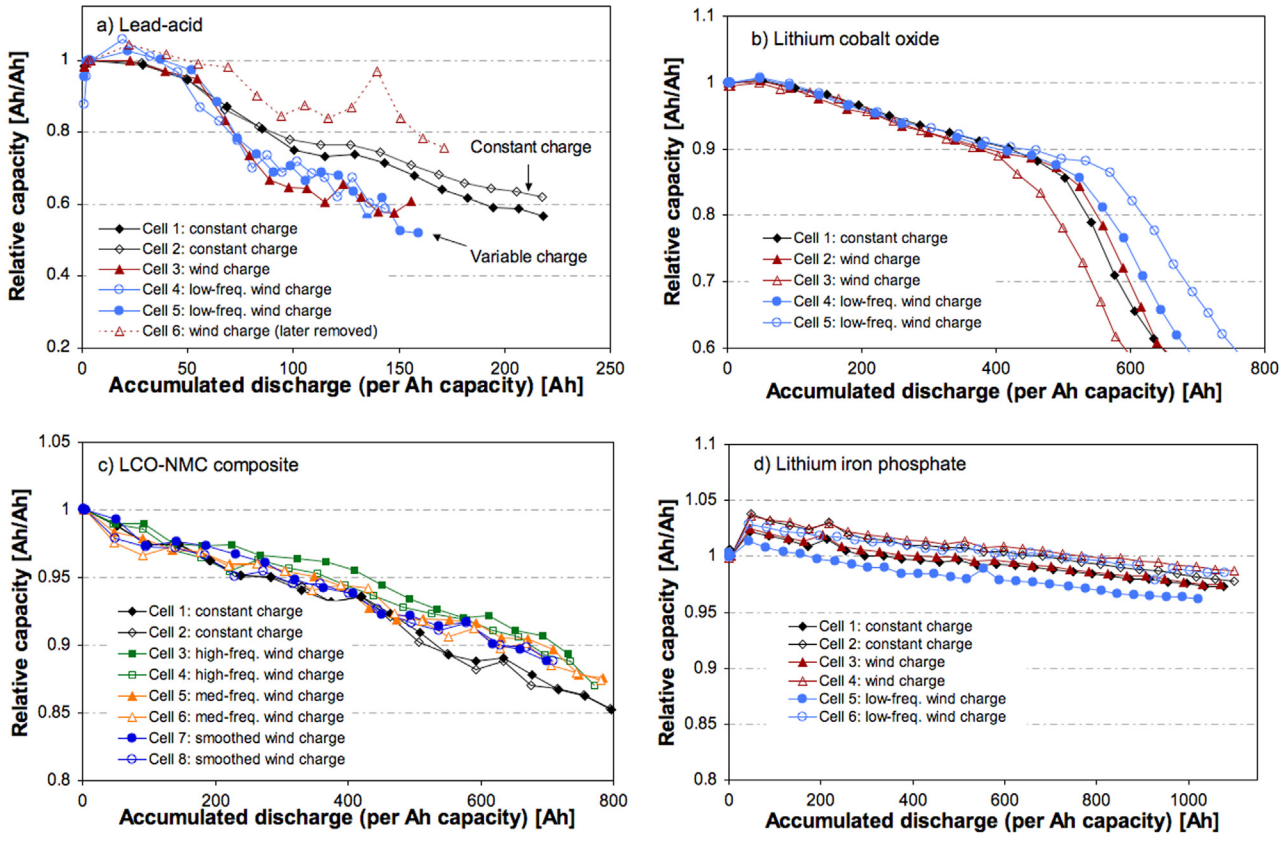

Fig. 2. Capacity fade as a function of normalized discharge throughput in a) lead-acid, b) LCO c) LCO-NMC and d) LFP cells.

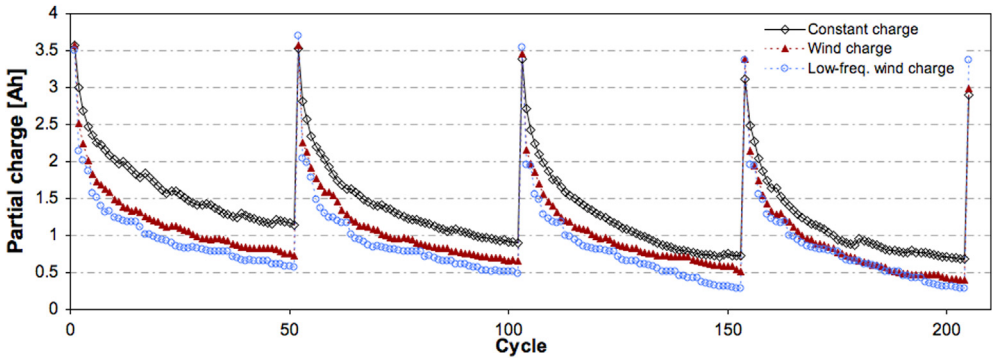

Fig. 3. Partial charging as a function of cycle for lead-acid cells charged with constant, standard wind or low-frequency wind protocols.

4. Results and discussion

The effects of wind cycling on the batteries are first evaluated by measuring capacity fade, second by evaluating pulse charge acceptance and power fade, and finally by using non-invasive differential capacity analysis to assess material degradation mechanisms.

4.1. Capacity fade

The capacity of the third characterization cycle is used as the baseline capacity of all tested cells. Given values are measured at a *C*/3 discharge rate. The initial lead-acid cell capacity ranged from 3.50 to 3.58 Ah, with the exception of one 3.68 Ah cell which remained an erratic outlier for the remainder of the cycling tests and is not considered in the final analysis. The capacity of the LFP cells ranged from 2.0 Ah to 2.08 Ah. The LCO cells ranged from 2.18 to 2.20 Ah. The LCO-NMC cells ranged from 2.12 Ah to 2.14 Ah. Subsequent capacity loss is measured in relation to these initial values.

Cell capacity is measured after every 50 cycles. The full cell capacity cannot be determined during each cycle set because the test cycles omit a constant voltage step, leaving the cells only partially charged. The degree of partial charging varies with charging protocol and over the course of each cycle set, rendering cycle number a somewhat misleading measure of time. Relative capacity fade is plotted as a function of the battery's accumulated discharge in Ah divided by cell capacity. This normalization allows for comparison between battery chemistries with different cell capacities.

Capacity fade in the lead-acid cells as a function of normalized accumulated discharge Ah is given in Fig. 2a. The cells show a significant amount of variation, which we attribute to both internal characteristics as well as fluctuations in ambient lab temperature. One cell charged with the standard wind profile exhibits erratic behavior and, while plotted in Fig. 2a, is not considered in

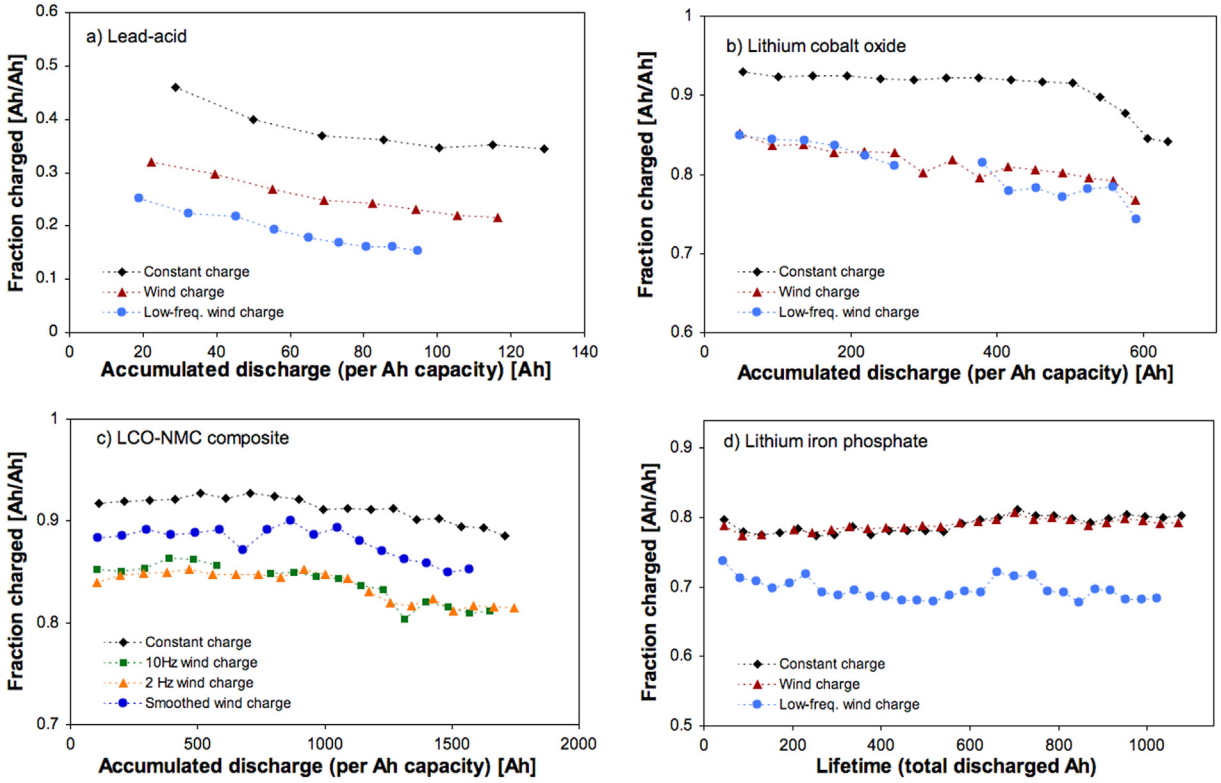

Fig. 4. Partial charging measuring charge power fade in a) lead-acid, b) LCO, c) LCO-NMC and d) LFP cells.

subsequent analysis. The cells charged at a constant rate show less degradation per processed Ah than the cells charged at a variable rate with the wind and low-frequency wind profiles. All cells reach 80% capacity after about 75–90 discharged Ah per Ah installed, but lead-acid cells in off-grid renewable systems are typically used beyond this standard "end of life" measure. Both wind-charged protocols age the cells similarly, but these cells reach 60% capacity after only about 2/3 of the Ah throughput that the constant charge cells can process before degrading to the same capacity.

A couple of factors may contribute to the better life performance of the constant-charge cells. The wind-charged cells were less fully charged (i.e. more undercharged) than constant-charge cells due to earlier arrival at voltage charge limits, a result of the high-current charging pulses (see Ref. [36]); such incomplete full charge typically contributes to sulfate crystal growth [15]. Cells are subject to high current pulses, which may help inhibit large crystal growth [29], but which may also contribute to overpotential and side reactions. The greater degree of partial cycling in the wind-charged cells means that they are actually fully charged more frequently than the constant-charge cells in calendar time, but these full charges only partially reverse the capacity fade in these cells. The accelerated conditions of this study contribute to higher degradation rates than expected for typical off-grid usage, but the results reflect the negative impact of partial charging and variability.

Unlike the lead-acid cells, the LCO and LCO-NMC cells show no aging benefit from the constant-charge profile. In Fig. 2b, LCO cells charged with the low-frequency wind profile show the least capacity fade, but these results may be within the noise of the system. In Fig. 2c, the LCO-NMC cells charged at a constant rate appear to lose capacity faster than those charged with any of the wind-based profiles, but the degradation trends have yet to fully differentiate after only 15% capacity loss. If this effect is real, it may be ascribed in part to the less complete charging of the wind-aged batteries. Li-ion batteries tend to degrade faster at higher SOC [37,38] and so may actually benefit from partial cycling. The LCO-NMC cells last much longer than the LCO cells: the LCO batteries reach 80% capacity after 600–700 cycles (500–650 Ah normalized throughput), whereas the LCO-NMC batteries retain nearly 90% of capacity after the same number of cycles.

The LFP cells, shown in Fig. 2d, show little aging after over 1200 cycles and nearly 1000 processed Ah per installed Ah. Capacity fade ranges from 1% to 3% loss from initial capacity. While the cells vary in total measured capacity fade, this variance does not appear correlated with charge protocols and occurs primarily over the first fifty cycles; after this point, the degradation rate of all cells are similar. The variance may stem from different charge histories during production. No variation in capacity fade between charge protocols could be identified from these plots. While the LCO and LCO-NMC chemistries both exhibit significantly slower rates of capacity fade than the lead-acid cells, the LFP cells degrade at a fraction of the rate of the other chemistries under both variable and constant charge.

4.2. Partial charging

The charging protocol used results in incomplete full charge during cycling due to charge ending at a prescribed voltage limit

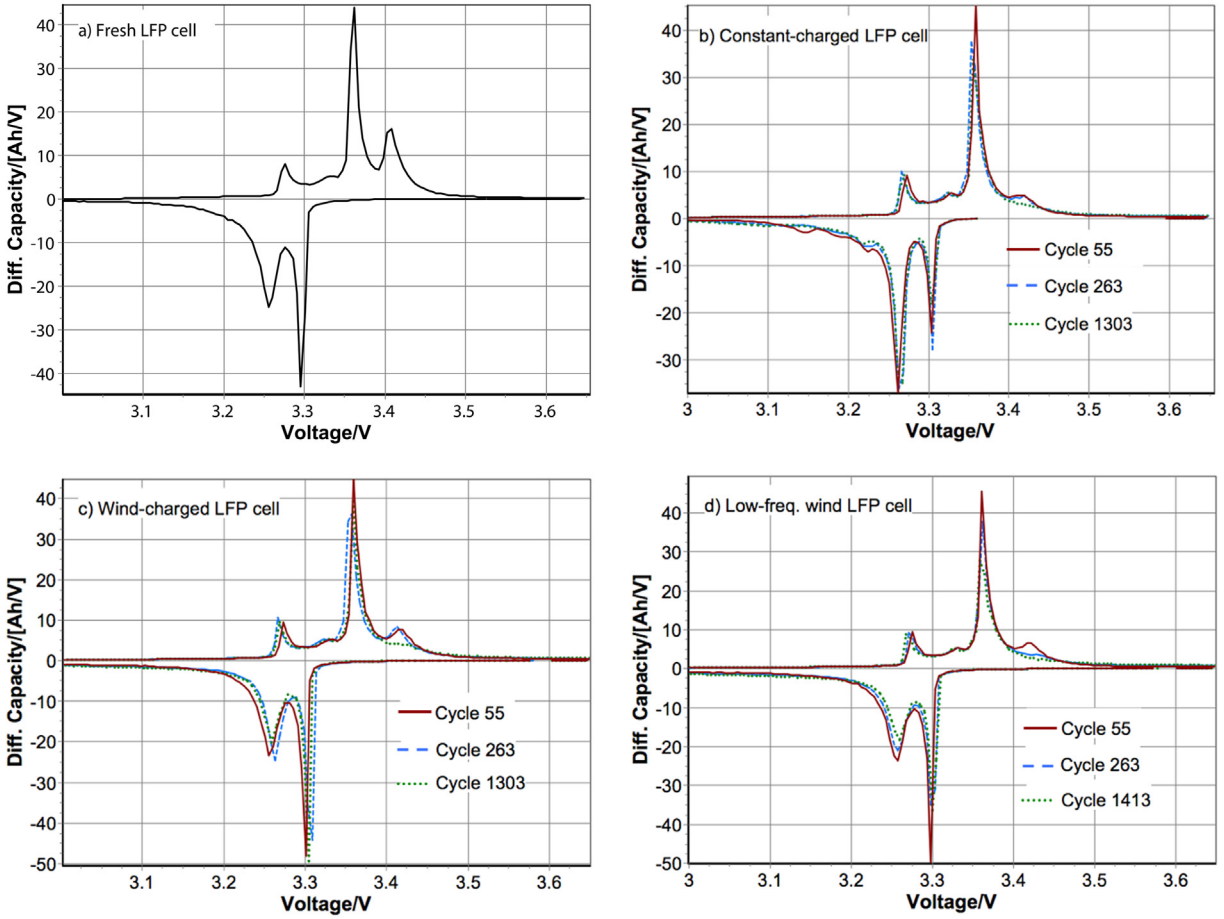

Fig. 5. LFP differential capacity plots for a) fresh, b) constant-charged, c) wind-charged and d) low-frequency wind-charged cells.

without being followed by a constant voltage step. Partial charge is characteristic of storage in off-grid renewable systems, so this characteristic of the test reflects an important stressor in off-grid conditions. However, in order to differentiate between the impact of the charging profile itself on aging and the impact of incomplete charging, we must characterize the degree of partial charging in each test.

In the lead-acid cells, the first partial charge after a full capacity test is the most complete, with decreasing capacity on each partial charge (increasing undercharge) over the next fifty cycles. Effectively, the battery has less available capacity to be charged in each successive cycle without a CV step. This effect is shown in Fig. 3, which plots the amount of charge (Ah) per cycle for the constant, standard wind, and low-frequency wind charging protocols. We see two major trends in the data. The charge starts relatively high after each CV step, then drops off precipitously for each subsequent step; much of this "loss" disappears after the next CV step, suggesting that this effect is due in part to reversible capacity fade. We attribute this effect to an increase in sulphation, reducing the amount of available active material, which is partially reversed during the CV step [39]. We note here that the LCO and LCO-NMC cells do not exhibit the reversible capacity fade observed in the lead-acid cells, but that the LFP cells show a slight increase in capacity after CV charge, which has been remarked on in Ref. [40].

The second trend we notice is that the batteries accept more charge at a constant rate than variable, and at a 1 Hz frequency than 0.1 Hz. The high current pulses increase overpotential, causing the wind-charged batteries to reach their voltage limit rapidly, cutting off voltage earlier than constant charge. Furthermore, the 10 s pulses result in more overpotential than the 1 s pulses, so the low-frequency wind profile reaches these voltage limits earlier than the standard wind profile.

The amount of charge in each aging cycle is a function of both capacity fade and power fade. Capacity fade determines the upper limit to the cell capacity using an optimal charge strategy, and power fade reflects the decreasing ability of the cell to charge or discharge at high currents. In order to differentiate between these two effects, we plotted the amount of partial cycling (in Ah) divided by the average of the full capacity at that time as determined by the CC–CV capacity cycles. In Fig. 4, we plot the average charge per set of 50 cycles, divided by the average of the full capacity tests at the beginning and end of the set. By dividing by the current capacity, any trends we see are indicative of the battery's ability to charge under the given protocol. These plots are effectively a measure of *partial charging* as a function of time and protocol. The rate-dependence of partial charging is described in detail in Ref. [36].

We can see two key pieces of information in these plots: 1) the amount each battery can be charged under each protocol (i.e. the measure of partial charge in Ah), and 2) the change in the amount of partial charging over time. In the lead-acid batteries in Fig. 4a, as we observed in Fig. 3, we see that the constant protocol charges the most, followed by the standard wind and low-frequency wind, suggesting pulse charge acceptance is greater for 1 s pulses than 10 s pulses. Furthermore, all protocols show a decline over time. This result is potentially symptomatic of increased internal resistance and power fade: the batteries have capacity that can be

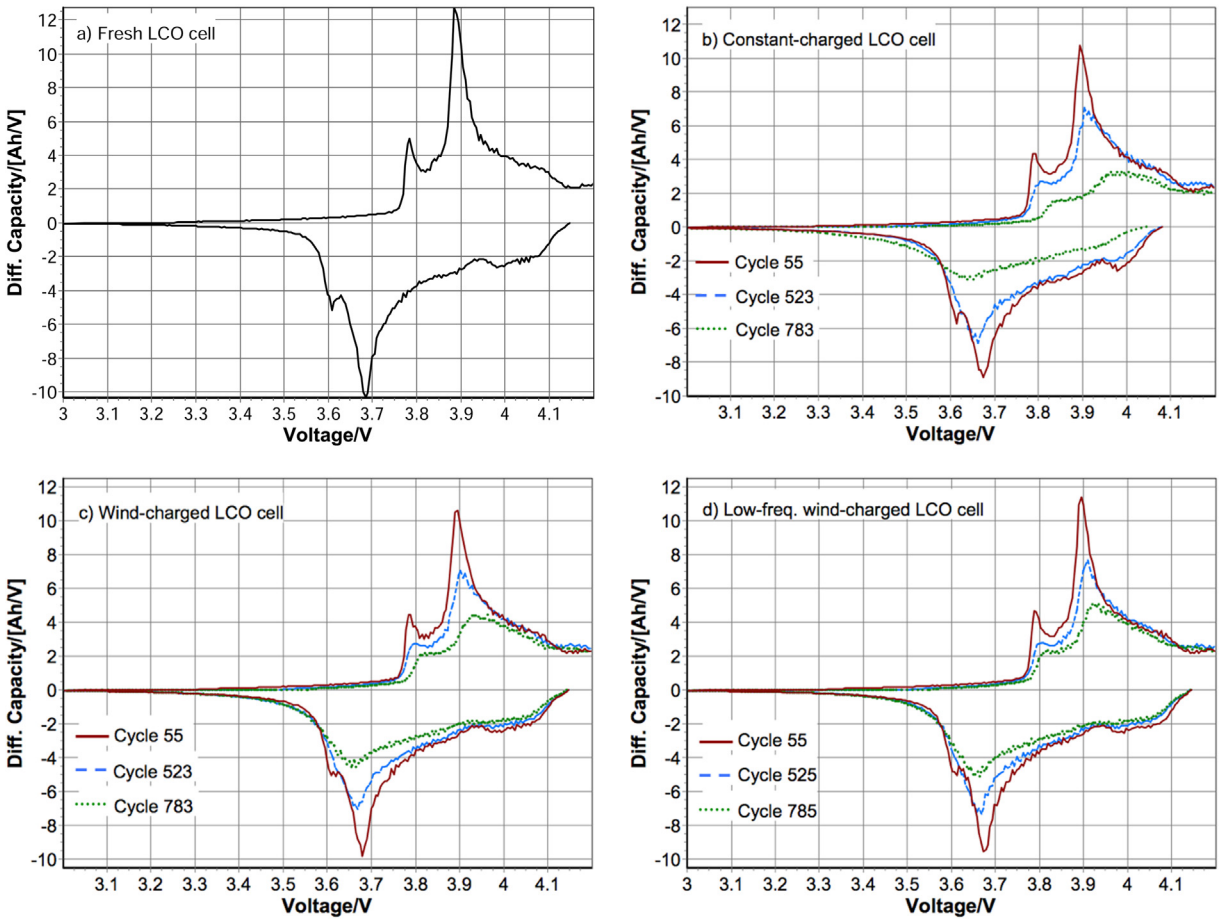

Fig. 6. LCO differential capacity plots for a) fresh, b) constant-charged, c) wind-charged and d) low-frequency wind-charged cells.

charged, but over time the full capacity may only be available at low charge powers. The lead-acid cells show much greater undercharge under all protocols than the other chemistries.

In the LCO and LCO-NMC batteries in Fig. 4b and c we also see better charge acceptance for constant than variable wind-based charging. However, in the LCO cells we observe no difference in charge acceptance between the low-frequency and standard wind protocols, and in the LCO-NMC cells frequency also does not appear to impact charge acceptance at the frequencies tested. All tested LCO and LCO-NMC cells show much greater charge acceptance for variable charge than the lead-acid cells, particularly for variable charge protocols.

In the LFP cells in Fig. 4d, the constant and standard wind cycles show the *same* level of partial charging, and only the low-frequency wind cycles with 10 s pulses show a lower amount of charge per cycle. Unlike in the other lithium-ion chemistries, charge acceptance appears to depend on pulse length in the range tested. Over time, LFP cells show relatively consistent levels of partial charging. The relatively constant power performance of these cells is consistent with the hypothesis that the primary degradation mechanism in these cells is loss of active material (cyclable lithium and graphite) as opposed to ohmic losses due to resistance increase [41], so there is little evidence of power fade.

Overall, the LCO and LCO-NMC cells show more complete charge at constant than variable rates, but the wind-charged LFP cells exhibit the same charge acceptance as constant-charge cells. LCO and LCO-NMC charge acceptance does not vary with the frequencies tested, whereas charge acceptance in the lead-acid and LFP cells is worse for longer pulses due to an increase in overpotential. The lead-acid, LCO-NMC and LCO cells show a decreasing ability to accept charge over time, even after normalizing for capacity fade; we attribute this result to increasing internal resistance and power fade. The lead-acid cells also show high levels of reversible capacity loss; while this capacity can be returned upon full charge, it suggests that after a few cycles of undercharge, typical in off-grid applications, the charging capacity of these cells is severely limited. The LFP batteries show no such power fade.

4.3. Electrochemical aspects of capacity fade

The physical mechanisms behind the capacity fade in the batteries are probed by looking at the differential capacity curves for each cell. Differential capacity illustrates the change in capacity dQ/dV as a function of voltage V. Peaks in the differential capacity curves are indicative of plateaus in the charge/discharge curves, and as such can be traced to material changes during charge and discharge. The method allows for studies of battery degradation mechanisms in a non-destructive manner, as has been demonstrated in Refs. [42,43]. Analysis is taken from the full capacity tests at a $C/3$ charge and discharge rate; this rate is too fast to capture all features but reflects the primary peaks.

We see the initial differential capacity plots for the LFP cells in Fig. 5a. The potential of the cathode is relatively smooth, so the peaks correspond to different stages of graphite lithiation [41,44]. Differential capacity plots after cycling are shown for constant-charged, wind-charged and low-frequency wind-charged cells in Fig. 5b, c, and d, respectively. Although resistance changes have been observed in previous studies [43], the peaks here have shown

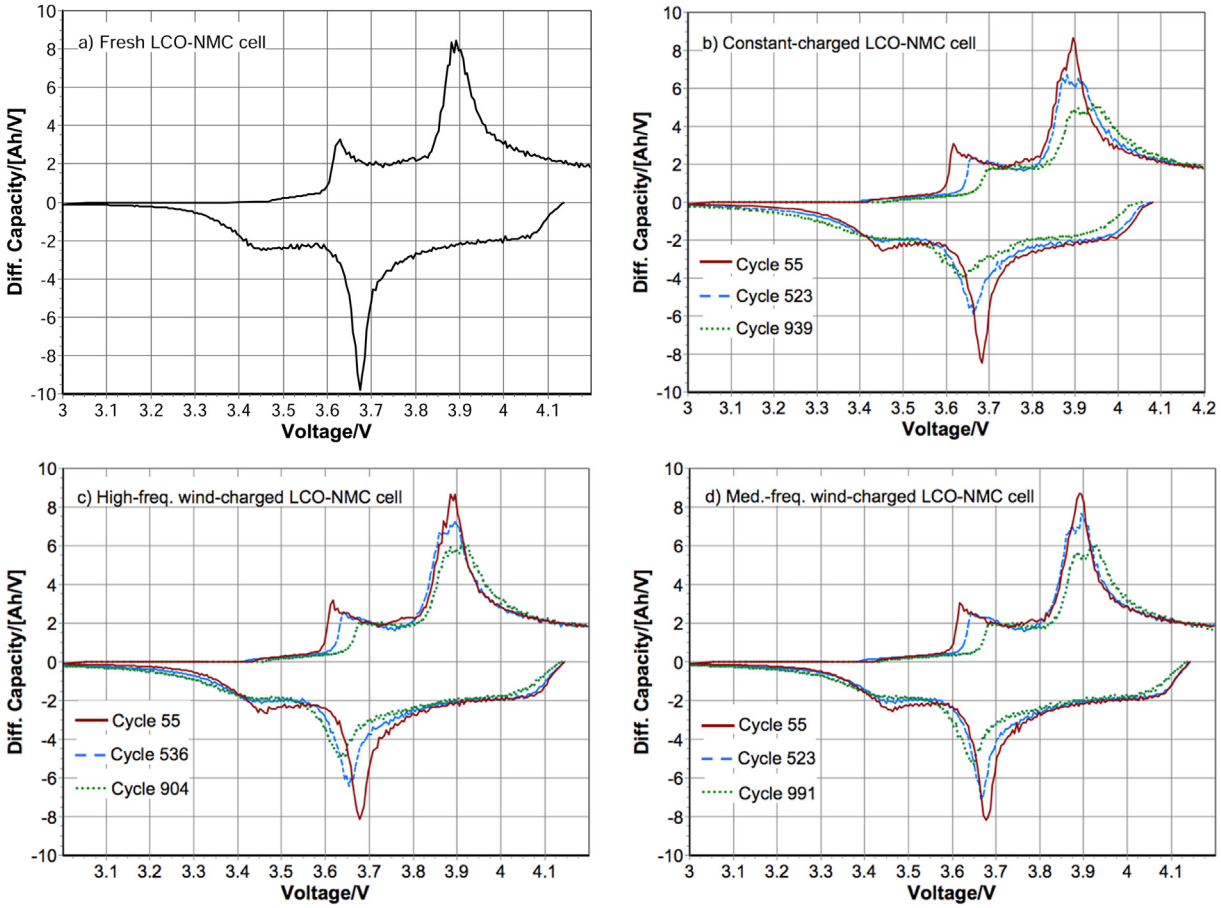

Fig. 7. LCO-NMC differential capacity plots for a) fresh, b) constant-charged, c) high-frequency (10 Hz) wind-charged and d) medium-frequency (2 Hz) wind-charged cells.

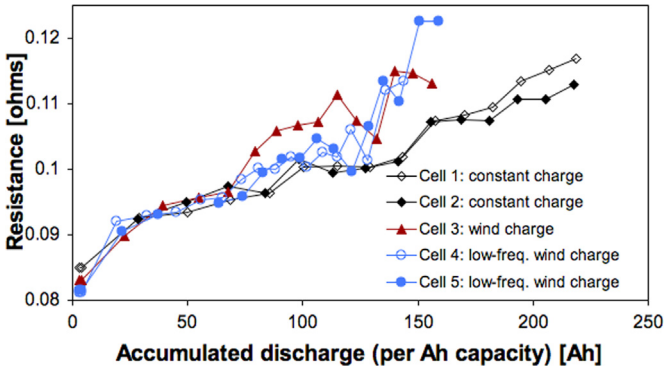

Fig. 8. Resistance calculated from pulse-charge tests at 100% SOC in lead-acid cells.

very little shift in location, indicating that there has been little increase in internal resistance in these cells. The third charging peak is observed to disappear with cycling in all LFP cells, although it disappears faster in the two low-frequency wind-charged cells, one of which is plotted in Fig. 5d. The third charging peak corresponds to the portion of the stage 1 graphite plateau that overlaps with the flat region of the LFP potential, and its disappearance suggests loss of cyclable lithium through irreversible side reactions. While the reason for the accelerated disappearance of the peak in the low frequency wind-charged cells is unknown, we saw in Section 4.2 that these cells are subject to more partial charging than the cells charged under other protocols. The loss of the third peak in all cells may indicate slight capacity fade, but this loss is too small to have been observed in Fig. 2d and only identifiable in the dQ/dV curves. The unequal loss among peaks is indicative of a loss of cyclable lithium [17,43]. The other peaks show a slight decrease in height, suggesting an overall loss in active material or cyclable lithium. The constant-charge cell shows a shift in intensity between its two primary discharge peaks (an effect also observed in the other constant-charge cell), which may indicate an overall shift in the operating window of this cell to lower voltage [41]. This shift occurs in the first fifty cycles, which we note in Fig. 5d is the period during which capacity variance is introduced in the LFP cells. The cause of this shift in peak intensity requires further research to fully explain.

Differential capacity plots for the LCO cells have more complicated features than the LFP cells (some of which cannot be observed at a C/3 rate), but some information can still be obtained from dQ/dV analysis. The differential capacity plot for a fresh LCO cell in Fig. 6a shows two primary peaks and a right shoulder. The first is a feature of stage 3 graphite in the anode overlapping with a relatively flat section of the cathode potential, and the second results from a combination of the dominant lithium insertion/extraction peak described in Refs. [45,46] and stage 2 graphite. The aging plots shown in Fig. 6b, c, and d all show a decrease in peak height, indicating loss in active material, and a shift to the right on the charge curves, reflecting increasing resistance. The low-frequency wind-charged cells show the least decrease in peak height, consistent with the lowest rate of capacity fade seen in Fig. 2b. The aged LCO-NMC cells in Fig. 7b, c, and d exhibit similar trends, including a decrease in peak height and resistive shift to the right; these degradation effects are strongest in the constant-charge cells, consistent with the faster degradation rates seen in Fig. 2c.

Differential capacity curves for the lead-acid cells show fewer distinct features than the lithium-based chemistries. We instead look at the resistance pulse tests taken after every fifty cycles. The internal resistance, calculated using Ohm's law from a 10 s charge pulse at 100% SOC, is shown as a function of normalized discharge throughput in Fig. 8. All cells show increasing resistance, but at high SOC the increase resulting from the variable charge protocols is greater than that from constant charging.

5. Conclusion

This study presents a comparison of lead-acid, LCO-NMC, LCO and LFP cell degradation when charged with a wind-based current profile to evaluate the impact of variability on cell aging and consider alternative battery chemistries for off-grid renewable projects. The lead-acid cells studied show rapid capacity fade characterized by an increase in internal resistance and loss of active material, with more rapid degradation in wind-charged cells than constant-charged cells. The lead-acid cells are also subject to severe partial charging when charged with a variable current; this latter effect is greater for longer pulses and reflects the poor pulse charge acceptance of these cells. The resultant incomplete charge is believed to accelerate sulphation and capacity fade. The LCO cells show better overall charge acceptance and, while variable charge results in greater partial charging, the frequency of the variability does not affect charge acceptance. Variability does not increase capacity fade in the LCO cells. The LCO-NMC cells degrade slower than the LCO cells, and constant charge cells show initial signs of faster degradation than variable charge cells, which may be the result of incomplete charging limiting the side reactions induced by high SOC. Degradation in the LCO-NMC cells appears to be initially due to loss of active material, but ultimately shows an increase in resistance as well. The LFP cells show very little degradation under all charging protocols. No increase in resistance is seen, and the slight reduction in capacity observed appears to primarily stem from the loss of cyclable lithium. Partial charging in these cells does depend on pulse frequency, and 1 s pulses are found to have greater charge acceptance than 10 s pulses. These results are summarized in Table 2.

LFP cells appear well-suited for off-grid renewable applications. The LFP cells not only show the least degradation under variable charging protocols, which are characteristic of all off-grid renewable energy generation, but the best voltage performance as well. Not only are their voltage curves flat, but their consistently low resistance means that as the batteries age, their power capability is relatively constant and they can still accept pulse charge without a large change in voltage or efficiency. Importantly, their ability to be charged at variable rates is consistently good over time. Their long lifetime would reduce the frequency of battery replacement in wind or solar systems. Their voltage performance suggests that

Table 2
Summary of battery response to variable charging.

Characteristic	Relevant figures	Lead-acid	LCO	LCO-NMC	LFP
Characteristic cycle life	Fig. 2	Poor	Good	Very good	Excellent
Effect of variability on lifetime	Fig. 2	Decreases lifetime	No measured effect	Neutral or positive effect	No measured effect
Pulse length dependence on charge acceptance	Figs. 3 and 4	Short pulses better than longer pulses	No measured effect	No measured effect	Short pulses better than longer pulses
Incomplete charge is a stressor	Fig. 3	Yes	No	No	No
Charge power fade observed	Fig. 4	Yes	Yes	Yes	No

they can continue to accept variable charge and meet variable demand over time. Deep discharge and incomplete charging, common off-grid stressors which accelerate aging in lead-acid cells, seem to have little impact on aging in these cells. As a result, battery systems for off-grid renewables could be sized much smaller for LFP cells. Typical lead-acid battery packs are sized for only 50% DOD, but a LFP pack could operate over the full range without accelerating aging and could be sized without needing to account for large future capacity loss. The LFP electrode is also much more stable and therefore safer than LCO-NMC and LCO cells.

Capital costs are relatively high for LFP batteries compared to lead-acid cells, which can already account for a significant portion of the cost of standalone renewable energy systems [8]. Even at current cost, however, this study suggests that LFP cells merit consideration in off-grid applications. A 12 V LFP pack can be purchased for $0.90/Wh, and 12 V lead-acid packs of the same size for $0.23/Wh. Assuming that the LFP pack need only be half the size of the lead-acid cell, it will be cost-competitive if it lasts just twice as long. Similar conclusions are likely to hold for large-scale grid-integrated intermittent renewable energy systems, which like off-grid standalone systems, require significant energy storage capacity for reliability [47–49]. While the accelerated testing conditions evaluated here cannot be translated directly to the field to compare aging rates, these studies suggest that LFP batteries may last many times longer than lead-acid cells in off-grid wind and solar applications and have significant potential to reduce energy storage costs over the lifetime of intermittent renewable energy systems. These cells also do not require the regular recharge needed to reverse sulphation in lead-acid cells, reducing maintenance. All of the lithium-based battery chemistries show less capacity fade and better performance in accelerated wind-charged conditions than lead-acid batteries, but the long lifespan and good voltage performance of LFP cells suggest they are well-suited for off-grid renewable energy systems.

Acknowledgments

We would like to thank the Carbon Mitigation Initiative at Princeton University and the National Science Foundation Graduate Research Fellowship for providing support for this work. Many thanks to Elie Bou-Zeid for providing us with wind data.

References

[1] IEA. World energy outlook 2012. OECD/IEA; 2012.
[2] IEA. Energy poverty: how to make modern energy access universal. OECD/IEA; 2010.
[3] Nandi S, Ghosh H. Energy 2010;35:3040–7.
[4] Perera A, Attalage R, Perera K, Dassanayake V. Energy 2013;54:220–30.
[5] Lau K, Yousof M, Arshad S, Anwari M, Yatim A. Energy 2010;35:3245–55.
[6] Jakhrani AQ, Othman A-K, Rigit ARH, Samo SR, Kamboh SA. Energy 2012;46:675–82.
[7] Dali M, Belhadj J, Roboam X. Energy 2010;35:2587–95.
[8] Kaldellis J, Zafirakis D, Kondili E. Energy 2009;34:1187–98.
[9] Gustavsson M, Mtonga D. Sol Energy 2005;79:551–8.
[10] Díaz P, Lorenzo E. Prog Photovolt Res Appl 2001;9:363–77.
[11] Okou R, Sebitosi A, Pillay P. Energy 2011;36:6138–45.
[12] Avril S, Arnaud G, Florentin A, Vinard M. Energy 2010;35:5300–8.
[13] Svoboda V, Wenzl H, Kaiser R, Jossen A, Baring-Gould I, Manwell J, et al. Sol Energy 2007;81:1409–25.
[14] Potteau E, Desmettre D, Mattera F, Bach O, Martin J, Malbranche P. J Power Sources 2003;113:408–13.
[15] Wenzl H, Baring-Gould I, Kaiser R, Liaw B, Lundsager P, Manwell J, et al. J Power Sources 2005;144:373–84.
[16] Spotnitz R. J Power Sources 2003;113:72–80.
[17] Safari M, Delacourt C. J Electrochem Soc 2011;158:A1123–35.
[18] Peterson SB, Apt J, Whitacre J. J Power Sources 2010;195:2385–92.
[19] Kim J, Woo S, Park M, Kim K, Yim T, Kim J, et al. J Power Sources 2013;229:190–7.
[20] Tofighi A, Kalantar M. Renew Energy 2011;36:2440–50.
[21] Gibson T, Kelly N. J Power Sources 2010;195:3928–32.
[22] Krebs F, Nielsen T, Fyenbo J, Wadstrøm M, Pedersen M. Energy Environ Sci 2010;3:512–25.
[23] Goemaere L, Soares A, Ionica-Bousquet C, Thiaux Y, Stievano L, Glaize C, et al. J Power Sources 2011;196:8688–91.
[24] Bindner H, Cronin T, Lundsager P, Manwell J, Abdulwahid U, Baring-Gould I. Benchmarking 2005;12:82.
[25] Wagner R, Sauer D. J Power Sources 2001;95:141–52.
[26] Baring-Gould I, Newcomb C, Corbus D, Kalidas R. Field performance of hybrid power systems. National Renewable Energy Laboratory; 2001.
[27] Corbus D, Newcomb C, Baring-Gould E, Friedly S. AWEA WINDPOWER 2002 Conference.
[28] Okazaki S, Higuchi S, Nakamura O, Takahashi S. J Appl Electrochem 1986;16:894–8.
[29] Lam L, Ozgun H, Lim O, Hamilton J, Vu L, Vella D, et al. J Power Sources 1995;53:215–28.
[30] Kirchev A, Mattera F, Lemaire E, Dong K. J Power Sources 2009;191:82–90.
[31] Kirchev A, Perrin M, Lemaire E, Karoui F, Mattera F. J Power Sources 2008;177:217–25.
[32] Pavlov D, Petkova G, Dimitrov M, Shiomi M, Tsubota M. J Power Sources 2000;87:39–56.
[33] Savoye F, Venet P, Millet M, Groot J. IEEE Trans Ind Electron 2012;59:3481–8.
[34] Chen L, Wu S, Shieh D, Chen T. IEEE Trans Ind Electron 2013;60:88–97.
[35] Berndt D. J Power Sources 2001;100:29–46.
[36] Krieger E, Arnold C. J Power Sources 2012;210:286–91.
[37] Choi S, Lim H. J Power Sources 2002;111:130–6.
[38] Vetter J, Novak P, Wagner M, Veit C, Möller K, Besenhard J, et al. J Power Sources 2005;147:269–81.
[39] Schiffer J, Sauer D, Bindner H, Cronin T, Lundsager P, Kaiser R. J Power Sources 2007;168:66–78.
[40] Hund T, Ingersoll D. Sandia National Laboratories, unlimited release; 2008.
[41] Kassem M, Bernard J, Revel R, Pélissier S, Duclaud F, Delacourt C. J Power Sources 2012;208:296–305.
[42] Dubarry M, Svoboda V, Hwu R, Liaw B. J Power Sources 2007;165:566–72.
[43] Dubarry M, Liaw B. J Power Sources 2009;194:541–9.
[44] Liu P, Wang J, Hicks-Garner J, Sherman E, Soukiazian S, Verbrugge M, et al. J Electrochem Soc 2010;157:A499–507.
[45] Reimers J, Dahn J. J Electrochem Soc 1992;139:2091–7.
[46] Barker J, Pynenburg R, Koksbang R, Saidi M. Electrochim Acta 1996;41:2481–8.
[47] Carton J, Olabi A. Energy 2010;35:4536–44.
[48] Lund H. Energy 2005;30:2402–12.
[49] Schenk NJ, Moll HC, Potting J, Benders RM. Energy 2007;32:1960–71.